Morphological Control *via* Chemical and Shear Forces in Block Copolymer Self-Assembly in the Lab-on-Chip

Chih-Wei Wang,[†] David Sinton,[‡] and Matthew G. Moffitt[†,*]

[†]Department of Chemistry, University of Victoria, P.O. Box 3065, Victoria, BC, Canada V8W 3V6 and [‡]Department of Mechanical and Industrial Engineering, University of Toronto, 5 King's College Road, Toronto, ON, Canada, M5S 3G8

ABSTRACT We investigate the effects of variation in chemical conditions (solvent composition, water content, polymer concentration, and added salt) on the morphologies formed by PS-*b*-PAA in DMF/dioxane/water mixtures in a two-phase gas–liquid segmented microfluidic reactor. The differences in morphologies between off-chip and on-chip self-assembly and on-chip morphological trends for different chemical conditions are explained by the interplay of top-down shear effects (coalescence and breakup) and bottom-up chemical forces. Using off-chip morphology results, we construct a water content-solvent composition phase diagram showing disordered, sphere, cylinder, and vesicle regions. On-chip morphologies are found to deviate from off-chip morphologies by three identified shear-induced paths: 1) sphere-to-cylinder, and 2) sphere-to-vesicle transitions, both *via* shear-induced coalescence when initial micelle sizes are small, and 3) cylinder-to-sphere transitions *via* shear-induced breakup when initial micelle sizes are large (high capillary number conditions). These pathways contribute to the generation of large extended bilayer aggregates uniquely on-chip, at either increased polymer or salt concentrations. Collectively these results demonstrate the broad utility of top-down directed molecular self-assembly in conjunction with chemical forces to control morphology and size of polymer colloids at the nanoscale.

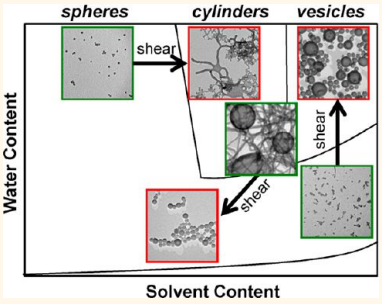

KEYWORDS: block copolymers · micelle morphologies · microfluidics · self-assembly · directed assembly · polymer vesicles

The solution self-assembly of block copolymers into colloidal nanostructures (termed block copolymer micelles) has inspired research in many corners of science and engineering, due to its fascinating parallels to spontaneous organization in living systems, along with its promising applications in materials science.[1−27] A central focus has been the understanding and control of the various micelle morphologies, including spheres, cylinders, and vesicles, since the size and shape of colloidal particles will profoundly influence their effectiveness for specific applications, including drug delivery,[28,29] sensing,[30] and medical imaging.[31−33]

Conventional morphological control over block copolymer self-assembly in solution is *via* intermolecular forces (i.*e.*, from the bottom-up), with variation of chemical parameters directly influencing the strength and nature of these forces and thus the structural products of self-assembly.[1−27] In particular, various groups have investigated the influence of block copolymer composition,[9,10,17] polymer concentration,[16,21] solvent,[14,20,27] pH, and ionic strength[11,16,22,34] on nanostructures obtained by block copolymer self-assembly. For example, Eisenberg and co-workers observed that polystyrene-*block*-poly(acrylic acid) (PS-*b*-PAA) micelle morphologies transformed from spheres, to cylinders, to vesicles as the THF content in mixtures of THF/DMF/water was increased, due to increased chain stretching as the core became increasingly swollen by the solvent (THF) with the higher PS affinity.[14,20,27] The same group showed that in similar systems of PS-*b*-PAA, adding various amounts of salt, acid or base led to dramatic differences in micelle morphologies, attributed to changes in the extent of electrostatic repulsion between PAA chains.[11,16,22,34] In many cases, these chemically induced morphological transformations are found to be reversible, suggesting that the structures are controlled by thermodynamics.[11,14,16,20,22,27,34] In fact, empirical equilibrium phase diagrams for block copolymer micelle morphologies as a function of chemical conditions have been determined.[13,16,21] However, under conditions where interfacial tension between the

* Address correspondence to mmoffitt@uvic.ca.

Received for review November 7, 2012 and accepted January 11, 2013.

Published online January 12, 2013
10.1021/nn305197m

microphase-separated blocks is extremely high, or chain dynamics are extremely slow, the sluggish reversibility of block copolymer self-assembly can lead to strong kinetic contributions to the observed micelle morphologies.[2,3,5]

In addition to the purely bottom-up approach, a small number of studies have employed forces external to the molecular system (*i.e.*, from the top-down), including shear and confinement, to partially direct the structural outcomes of block copolymer self-assembly.[35−41] Such strategies offer the potential for "dialing-in" desired morphologies through relatively simple changes in processing conditions without changes in chemical formulation. For example, our group has recently shown that the self-assembly of PS-*b*-PAA block copolymers on a multiphase gas−liquid microfluidic chip yields morphologies that are different from those produced under identical chemical conditions in the bulk (Figure 1).[40,41] In solvent mixtures of 75/25 (w/w) at different water contents, it was found that a PS-*b*-PAA copolymer that formed spheres in the bulk yielded mixtures of spheres and networks of mainly cylindrical micelles.[40] In a follow-up study, we showed that the same copolymer also forms spheres in pure dioxane and water, whereas on-chip the identical solution produced vesicles.[41] These results were explained by a two-part mechanism in which shear-induced collision/coalescence of thermodynamically stable micelle structures in the high-shear corners of the liquid plugs in the gas−liquid microfluidic reactors produced high free energy aggregates which then relax nonergodically to various kinetically stable morphologies *via* intramicellar chain rearrangements.[40,41] Either cylinders or vesicles were generated as a result of on-chip shear-induced processes, suggesting that the initial equilibrium state, dependent on the solvent environment, plays an important role in determining which morphological transformation pathways can be unlocked by on-chip shear. However, to date, the on-chip combination of molecular self-assembly and high shear, and the resulting morphological control, has been demonstrated only under a few isolated chemical conditions.

In this paper, we describe a systematic study of the influence of various chemical parameters on morphologies formed on-chip, with comparison to the structures formed off-chip under equivalent chemical conditions. Specifically, we quantify the effects of different solvent mixtures, water contents, polymer concentrations, and added salt. We show that these chemical parameters have a considerable influence on the thermodynamics and kinetics of on-chip micelle formation, which in turn governs the resulting micelle morphologies *via* an interplay between chemical and shear forces. Moreover, an improved understanding of chemical effects on shear-directed self-assembly processes on-chip expands the toolbox of block copolymer morphological control to include a new suite of flow-directed micelle manufacturing strategies involving microfluidic reactors.

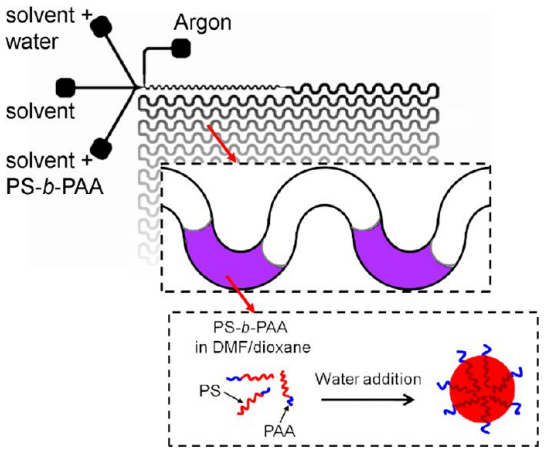

Figure 1. Schematic of the gas−liquid microfluidic reactor, with insets showing segmentation of gas and liquid (top) and PS-*b*-PAA self-assembly within the liquid plugs (bottom).

TABLE 1. Some Physical Parameters of Solvents and Polymers

material	solubility parameter (δ/[MPa]$^{1/2}$)	dielectric constant (ε)
DMF	24.8	38.2
dioxane	20.5	2.2
PS	18.7	

RESULTS AND DISCUSSION

Solvent Composition Dependence of PS-*b*-PAA Morphologies Formed Off-Chip. Before understanding the effect of solvent composition on the on-chip morphologies, it was first necessary to investigate the influence of solvent composition on off-chip morphologies of PS-*b*-PAA micelles, which in most cases represent equilibrium states. First, for the "crew-cut" copolymer employed in this study, PS(665)-*b*-PAA(68), critical water contents in various mixtures of DMF/dioxanes were determined. The relevant solubility parameters and dielectric constants for this system are given in Table 1. Clearly, as the dioxane content of DMF/dioxane increases, the solubility parameter of the mixture will become closer to the value for the PS block, while the dielectric constant of the mixture will decrease. One result of the increased solvent quality for the PS block with increasing dioxane content is the concomitant increase in the critical water content (cwc) for micelle formation: as the PS blocks are more strongly solvated by the organic solvent, more water is required to precipitate them from the solvent phase.[16] This is shown by the results in Figure 2. The cwc values for PS(668)-*b*-PAA(65) in different DMF/dioxane compositions were carefully determined using the well-established light scattering technique, in which sharp increases in scattering intensity with increasing water content indicate the cwc (Figure 2A).[16] As shown in Figure 2B, the general trend of increasing cwc with

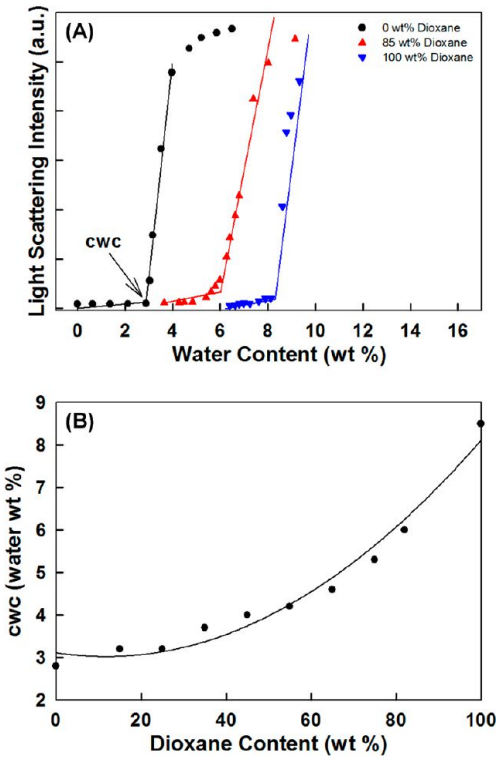

Figure 2. Critical water content (cwc) determination of PS-(665)-*b*-PAA(68) (c_0 = 0.33 wt %) in various DMF/dioxane mixed solvents. (A) Examples of cwc determinations in DMF, dioxane, and 15/85 (w/w) DMF/dioxane mixture using the static light scattering method described in the text. The cwc of the solution in DMF (2.8 ± 0.1 wt %) is indicated with an arrow. (B) Plot showing cwc as a function of dioxane content in various DMF/dioxane mixtures.

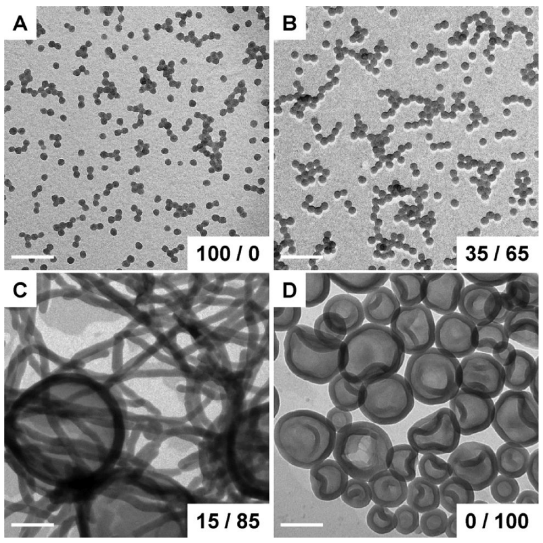

Figure 3. Effect of solvent composition on off-chip morphologies of PS(665)-*b*-PAA(68). TEM images of micelle morphologies formed from bulk (off-chip) self-assembly of PS(665)-*b*-PAA(68) (c_0 = 0.33 wt %) in various DMF/dioxane (w/w) mixtures: (A) 100/0 (pure DMF), (B) 35/65, (C) 15/85, and (D) 0/100 (pure dioxane). In all cases, the water content during self-assembly was cwc + 2 wt %. The scale bars indicate 200 nm.

increasing dioxane content is exhibited by the data, as expected based on the solubility parameters. Here, we retain the convention adopted previously of investigating self-assembly at three different water contents above the cwc for each solvent mixture:[40] cwc + 1, 2, and 4 wt %; however, due to the different cwc values for the different solvent systems (Figure 2B), the absolute water contents for self-assembly are different for each mixture of DMF/dioxane.

The effect of solvent composition on the resulting micelle morphologies is demonstrated in Figure 3, which shows TEM images for off-chip self-assembly in DMF/dioxane (w/w) mixtures of 100/0, 35/65, 15/85, and 0/100, each at a relative water content of cwc + 2 wt %, which is 4.8, 6.6, 7.3, and 10.5 wt %, respectively, for each solvent composition. At lower dioxane contents, the sole morphology is spherical (Figure 3A,B) with the mean size of spheres increasing from 33 ± 2 nm (Figure 3A) to 40 ± 2 nm (Figure 3B) as the dioxane content increases from DMF/dioxane compositions of 100/0 to 35/65. A further increase in the dioxane content to 15/85 transforms spherical micelles to long cylinders and vesicles (Figure 3C). Finally, the micelle morphology progresses to pure vesicles in the 0/100 case (pure dioxane, Figure 3D). The observed trends are consistent with the results for similar PS-*b*-PAA copolymers described in the literature, and can be explained by a combination of increased solvent swelling of the PS cores and decreased repulsion between PAA chains as the dioxane content of the solvent mixture increases.[14,20,27] The resulting increase in PS stretching first effects an increase in core diameter (Figure 3A,B), followed by a morphological transformation to micelles with progressively lower internal curvature: first to cylinders (Figure 3C) and then to vesicles (Figure 3D).

In addition to the specific mixtures described in Figure 3, we investigated the morphologies obtained for a series of solvent mixtures between and including DMF/dioxane = 100/0 and 0/100, each at water contents of cwc + 1, 2, and 4 wt %. Table 2 compiles the main micelle morphologies observed in each of these cases. Spheres are observed at all water contents for solvent mixtures with dioxane contents up to and including 35/65. However, at dioxane contents of 25/75 and higher, cylinders and vesicles start to appear as the water content increases. In the 25/75 mixtures, the morphology is spherical at a water content of cwc + 1 wt %, although the increased thermodynamic driving force for micellization with an increase in water content to cwc + 2 wt % gives rise to a mixture of spheres and cylinders; the reversion to spheres as the water content further increases to cwc + 4 wt % is believed to be a kinetic effect, representing a trapped transition state due to the high core viscosity at the highest water content. For the 15/85 mixture, a similar transformation from spheres to a mixture of cylinders and vesicles occurs as the water

TABLE 2. Summary of Morphologies Formed *via* Off-Chip Self-Assembly[a]

DMF/dioxane (w/w) →	100/0	85/15	75/25	65/35	55/45	45/55	35/65	25/75	15/85	0/100
cwc/wt%	2.8	3.2	3.2	3.7	4.0	4.2	4.6	5.3	6.0	8.5
cwc + *x* wt %										
1.0	S	S	S	S	S	S	S	S	S	S + L
2.0	S	S	S	S	S	S	S	S + C	C + V	V
4.0	S	S	S	S	S	S	S	S*	S*+ V	V

[a] Notes: S = spheres and S* represent kinetically-trapped (nonequilibrium) spheres; C = cylinders; L = lamella; V = vesicles. The polymer concentration c_0 in all cases is 0.33 wt % and the cwc was determined using light scattering. The micelle morphologies were determined from TEM.

TABLE 3. Summary of Morphologies Formed *via* On-Chip Self-Assembly (Q = ~5 μL/min)[a]

DMF/dioxane (w/w) →	100/0	85/15	75/25	35/65	15/85	0/100
cwc/wt %	2.8	3.2	3.2	4.6	6.0	8.5
cwc + *x* wt %						
1.0	S	S	S + C	S + C (+ V)	S + V	V
2.0	S + C	S + C (+ L)	S + C (+ L)	S + C (+ V)	S + V	V
4.0	S	S	S	S (+ C)	S + V (+ C)	V (+ S)

[a] Notes: S = spheres; C = cylinders; L = lamella; V = vesicles. The polymer concentration c_0 in all cases is 0.33 wt % and the cwc was determined using light scattering. Minor morphologies are shown in brackets. The micelle morphologies were determined from TEM.

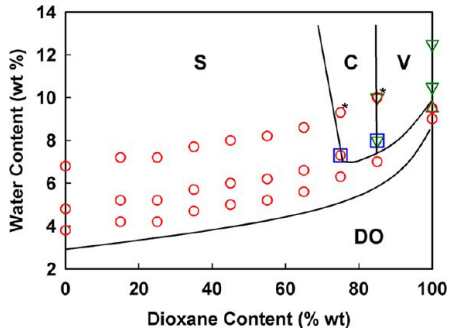

Figure 4. Water content−solvent composition phase diagram for PS(665)-*b*-PAA(68) (c_0 = 0.33 wt %), showing regions corresponding to unimers (disordered, DO), spheres (S), cylinders (C), and vesicles (V).

content increases from cwc + 1 wt % to cwc + 2 wt %. Further increasing water content to cwc + 4 wt % results in mostly smaller vesicles along with some spheres; again, the spheres are attributed to the high viscosity and slow chain dynamics at the highest water content, which precludes micelles from reaching their most thermodynamically favorable state. In pure dioxane (0/100), the transformation is from a mixture of spheres and lamellae (a structural precursor to vesicles) to pure vesicles as the water content increases from cwc + 1 wt % to cwc + 2 wt %, with mainly vesicles also observed at cwc + 4 wt %.

Considering that, for the most part (with exceptions noted in Table 2), the resulting off-chip self-assembled micelles should represent equilibrium morphologies, we used the data in Table 2 to construct a solvent composition *versus* water content phase diagram (Figure 4). The boundaries between morphological regions are estimated, and in the 25/75, cwc + 4 wt % case, where the observed spheres are believed to be a kinetically trapped transition state, the thermodynamic phase region is inferred from the general trends. The phase boundary between the unimer phase and the spherical phase is simply determined from the locus of cwc values described previously. This equilibrium phase diagram from off-chip self-assembly serves as an important starting point for understanding the nonequilibrium on-chip morphologies under various solvent conditions.

Solvent Composition Dependence of PS-*b*-PAA Morphologies Formed On-Chip. Our previous studies have suggested that shear processing of particles circulating through the strongly localized high-shear fields in the corners of the liquid plugs,[42] together with the chemical environment, are both important factors in on-chip morphologies.[40,41] Herein, we study on-chip self-assembly for various DMF/dioxane compositions and water contents of cwc + 1, 2, and 4 wt % in each solvent mixture. We compare the resulting on-chip micellar structures (Table 3) with morphologies formed under equilibrium conditions in the bulk under the corresponding chemical conditions (Table 2, Figure 4).

Along with the 75/25 DMF/dioxane system,[40] three other investigated compositions showed similar general trends in the relationship between bulk (off-chip) and on-chip micelle morphologies at different water contents. These are, in order of increasing dioxane content, 100/0 (pure DMF, Figure 5), 85/15 (Figure 6), 75/25 (Figure 7, represented for completeness) and 35/65 (Figure 8). Comparison of these figures shows that in all four DMF/dioxane mixtures, only spherical micelles were formed in the bulk at all investigated water contents, whereas cylindrical morphologies were generated on-chip at certain

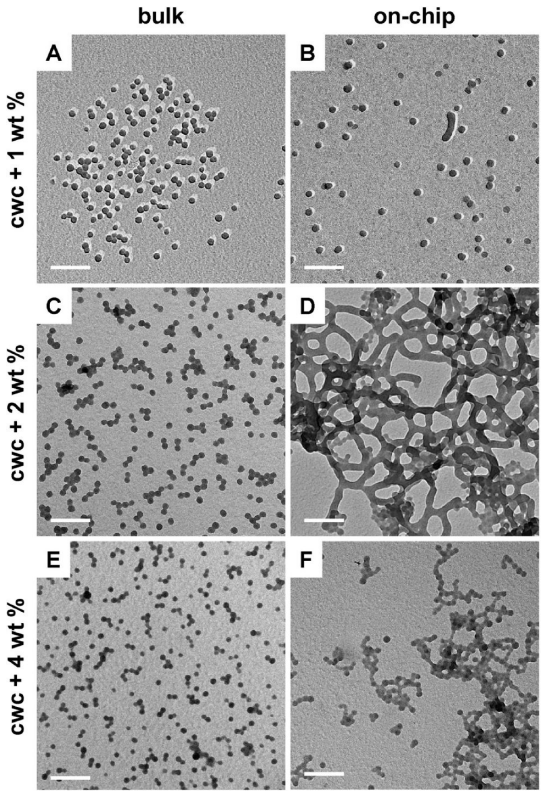

Figure 5. Effect of water content on off-chip and on-chip morphologies of PS(665)-*b*-PAA(68) in DMF. TEM images of micelle morphologies formed from bulk (A,C,E) and on-chip (B,D,F) self-assembly of PS(665)-*b*-PAA(68) (c_0 = 0.33 wt %) in DMF at water contents of cwc + 1.0 wt % (A,B), cwc + 2.0 wt % (C,D), and cwc + 4.0 wt % (E,F). For this solvent system, cwc = 2.8 ± 0.1 wt %. The on-chip flow rate is $Q = \sim 5\ \mu$L/min. The scale bars indicate 200 nm.

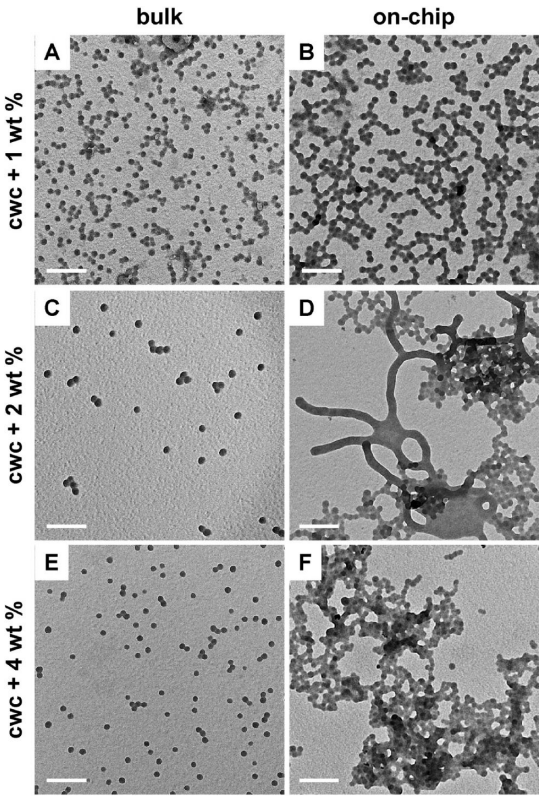

Figure 6. Effect of water content on off-chip and on-chip morphologies of PS(665)-*b*-PAA(68) in 85/15 (w/w) DMF/dioxane. TEM images of micelle morphologies formed from bulk (A,C,E) and on-chip (B,D,F) self-assembly of PS(665)-*b*-PAA(68) (c_0 = 0.33 wt %) in 85/15 (w/w) DMF/dioxane at water contents of cwc + 1.0 wt % (A,B), cwc + 2.0 wt % (C,D), and cwc + 4.0 wt % (E,F). For this solvent system, cwc = 3.2 ± 0.1 wt %. The on-chip flow rate is $Q = \sim 5\ \mu$L/min. The scale bars indicate 200 nm.

water contents. In the 100/0 (Figure 5) and 85/15 (Figure 6) mixtures, shear-directed cylinders are generated on-chip at cwc + 2 wt %, but not at cwc + 1 wt %; however, at higher dioxane contents, 75/25 (Figure 7) and 35/65 (Figure 8), on-chip cylinders formed at both cwc + 1 wt % and cwc + 2 wt %. All four solvent compositions formed only spheres on-chip at cwc + 4 wt %, although in most cases the resulting spheres appear to be highly aggregated compared to the bulk. The nature of the shear-induced morphologies is slightly different at the different solvent compositions, although all are dominated by cylindrical micelles: the 100/0 solvent forms only highly interconnected networks of cylinders (Figure 5D); the 85/15 (Figure 6D) and 75/25 (Figure 7B,D) mixtures form mainly branched and network cylinders, along with a few lamellae; the 35/65 (Figure 8B,D) mixture forms branched and network cylinders, along with a few vesicles.

Considering the equilibrium phase diagram based on off-chip morphologies (Figure 4), and the mechanism of on-chip morphology transformations proposed previously (Scheme 1),[40,41] we can understand why cylinders are the most prominent nonspherical structures generated in the microfluidic channel at the four compositions 100/0, 85/15, 75/25, and 35/65. In these mixtures, global equilibrium favors spheres, and so fast mixing with water generates spheres near the injector (Scheme 1, State A). Subsequent shear-induced coalescence of spheres in the high-shear corners of the liquid plugs locally increases aggregation numbers to generate high-energy aggregates (Scheme 1, State B). These transition structures then relax *via* the kinetically favored pathway of intramicellar chain rearrangements to form the morphology (Scheme 1, State C) that represents a local free energy minimum, within the kinetic constraint of local aggregation numbers in the absence of interparticle exchange.[2,3] Since the effect of shear-induced coalescence on-chip is to increase aggregation numbers,[40] it exerts a force locally that is morphogenically equivalent to the chemical force exerted by an increase in dioxane and/or water content (both of which will globally increase aggregation numbers). As a result, the equilibrium spheres are pushed by on-chip shear into the nearest morphological region with higher aggregation number, which is cylinders.

In Scheme 2, we superimpose the phase diagram of thermodynamically favored morphologies with the

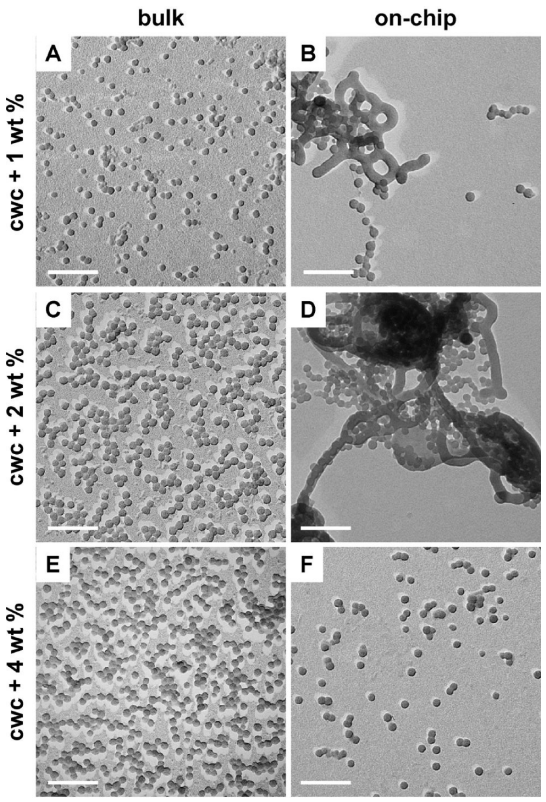

Figure 7. Effect of water content on off-chip and on-chip morphologies of PS(665)-*b*-PAA(68) in 75/25 (w/w) DMF/dioxane. TEM images of micelle morphologies formed from bulk (A,C,E) and on-chip (B,D,F) self-assembly of PS(665)-*b*-PAA(68) (c_0 = 0.33 wt %) in 75/25 (w/w) DMF/dioxane at water contents of cwc + 1.0 wt % (A,B), cwc + 2.0 wt % (C,D), and cwc + 4.0 wt % (E,F). For this solvent system, cwc =3.2 ± 0.1 wt %. The on-chip flow rate is Q = ~5 μL/min. The scale bars indicate 200 nm.

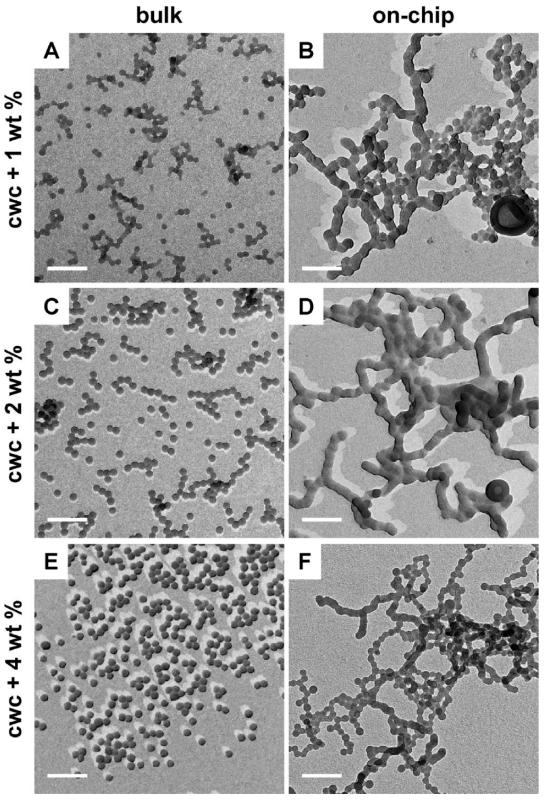

Figure 8. Effect of water content on off-chip and on-chip morphologies of PS(665)-*b*-PAA(68) in 35/65 (w/w) DMF/dioxane. TEM images of micelle morphologies formed from bulk (A,C,E) and on-chip (B,D,F) self-assembly of PS(665)-*b*-PAA(68) (c_0 = 0.33 wt %) in 35/65 (w/w) DMF/dioxane at water contents of cwc + 1.0 wt % (A,B), cwc + 2.0 wt % (C,D), and cwc + 4.0 wt % (E,F). For this solvent system, cwc = 4.6 ± 0.1 wt %. The on-chip flow rate is Q = ~5 μL/min. The scale bars indicate 200 nm.

various observed on-chip morphogenic transformations due to shear; in this classification of on-chip results, the process described above is represented by Path 1 (shear-induced coalescence from spheres, S, to cylinders, C). This analysis also explains why a small number of lamellae (a transition structure in vesicle formation, *e.g.*, Figure 6D) and then some vesicles (Figure 8B,D), are observed by on-chip self-assembly as the dioxane content increases; as the equilibrium composition moves closer to the sphere-cylinder phase boundary, a small number of particles will experience a sufficient increase in local aggregation number to undergo two morphogenic steps from spheres to cylinders to vesicles.

Under equilibrium (off-chip) conditions, the solvent composition 15/85 DMF/dioxane (Figure 9) lies in the sphere region just below the cylinder/vesicle phase boundary at cwc + 1 wt % (Figure 4, Figure 9A), and at different points along the cylinder/vesicle phase boundary at cwc + 2 wt % (Figure 9C) and cwc + 4 wt % (Figure 9E). As previously mentioned, the small number of spheres present along with vesicles at cwc + 4 wt % (Figure 9E), far from the equilibrium sphere

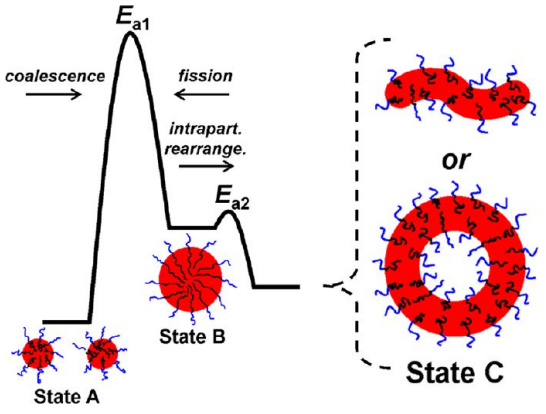

Scheme 1. Proposed energy diagram for on-chip morphological transitions *via* shear-induced coalescence and intraparticle chain rearrangements.

region, are believed to be kinetic structures trapped as a result of the high water content. On-chip, this solvent composition shows a rich variety of shear-induced morphogenic behavior that is strongly dependent on the water content and thus on the initial equilibrium morphologies that form immediately after the injector. At cwc + 1 wt %, where solely spheres are present

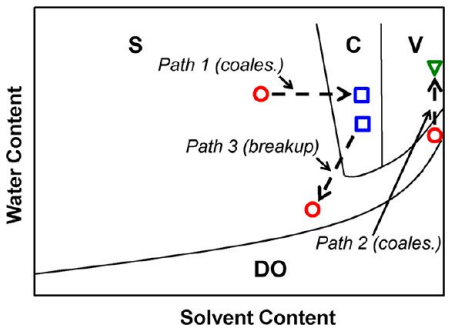

Scheme 2. Categorization of on-chip morphological transitions (dashed arrows) for different initial equilibrium conditions on the phase diagram. Paths 1 and 2 represent morphology transitions *via* shear-induced coalescence of spherical micelles (as described in Scheme 1). Path 3 represents a morphology transition *via* shear-induced breakup of cylinders to spheres; breakup rather than coalescence occurs in this case due to the high capillary number of the initially formed aggregates. Symbols represent initial and final states of various on-chip shear-induced pathways and do not correspond to specific data points.

under off-chip equilibrium conditions (Figure 9A), spheres along with a significant number of shear-induced vesicles, are formed on-chip (Figure 9B). The formation of shear-induced vesicles from equilibrium spheres, instead of the shear-induced cylinders observed at compositions with lower dioxane content, is attributed to the close proximity of spherical micelles under these conditions to the vesicle region of the phase diagram; thus, the local increases in aggregation number as a result of shear-induced coalescence push spherical aggregates into the vesicle region, as portrayed by Path 2 in Scheme 2.[41]

In contrast to the equilibrium spheres at cwc + 1 wt %, the chemical conditions at 15/85 DMF/dioxane and cwc + 2 wt % give rise to an equilibrium mixture of long cylinders and large vesicles off-chip (Figure 9C); on-chip, the dominant effect of downstream shear is particle breakup rather than coalescence. The predominance of on-chip shear-induced breakup at cwc + 2 wt %, in contrast to the predominance of shear-induced coalescence on-chip at cwc + 1 wt %, can be understood by comparing the equilibrium aggregates formed in the bulk under these two chemical conditions, which should be similar to the corresponding on-chip structures near the injector before significant exposure to shear. In general, the susceptibility of colloidal particles to breakup increases with the capillary number, Ca, which describes the balance of viscous to interfacial forces for dispersed liquid drops under shear:

$$\mathrm{Ca} = \frac{\eta_m \dot{\gamma} D}{2\Gamma} \quad (1)$$

where η_m is the viscosity of the matrix, $\dot{\gamma}$ is the shear rate, D is the particle diameter, and Γ is the dispersed phase/matrix phase interfacial tension. Therefore, compared to small spheres formed at cwc + 1 wt %, the larger sizes of the cylinders and vesicles formed upon mixing with

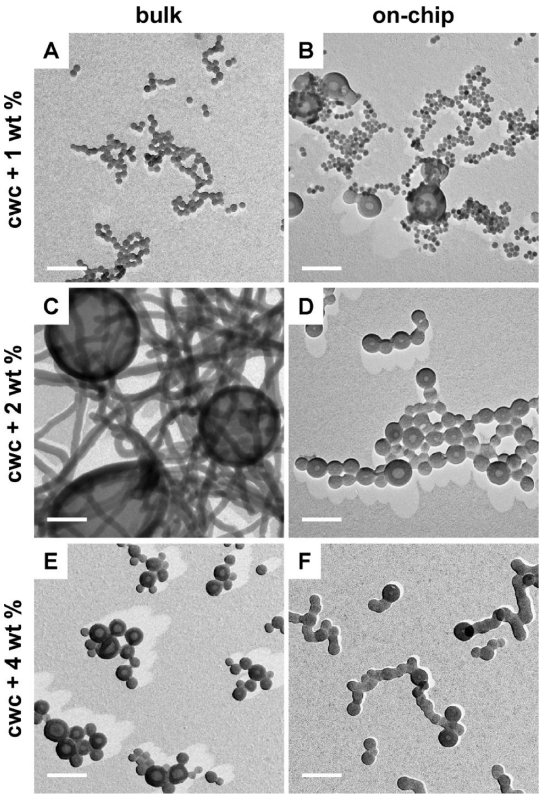

Figure 9. Effect of water content on off-chip and on-chip morphologies of PS(665)-*b*-PAA(68) in 15/85 (w/w) DMF/dioxane. TEM images of micelle morphologies formed from bulk (A,C,E) and on-chip (B,D,F) self-assembly of PS(665)-*b*-PAA(68) (c_0 = 0.33 wt %) in 15/85 (w/w) DMF/dioxane at water contents of cwc + 1.0 wt % (A,B), cwc + 2.0 wt % (C,D), and cwc + 4.0 wt % (E,F). For this solvent system, cwc = 6.0 ± 0.1 wt %. The on-chip flow rate is Q = ~5 μL/min. The scale bars indicate 200 nm.

water to cwc + 2 wt % leads to higher capillary numbers at the same shear rate, which increases their susceptibility to breakup.[40,42,43] Also, the high aspect ratio of the cylinders, and the low internal viscosities of the vesicles, will increase the rate of breakup relative to smaller, more compact spheres. As a result, the shear-induced on-chip morphologies (Figure 9D) have lower, rather than higher, aggregation numbers than their off-chip counterparts (Figure 9C), in the form of spheres and smaller vesicles. We represent this type of on-chip transition—from larger equilibrium aggregates (*e.g.*, cylinders) to smaller aggregates (*e.g.*, spheres) as a result of shear-induced breakup at high capillary number—by Path 3 in Scheme 2.

Finally, the cwc + 4 wt % morphologies on-chip (Figure 9F) and off-chip (Figure 9E) are consistent with other solvent compositions at high water content, in that the small particle size and large activation energy do not allow either significant breakup or coalescence under shear, such that the on-chip morphologies are not dramatically different from those formed off-chip under the same chemical conditions. However, we do note that a few cylindrical-like aggregates appear to form on-chip (Figure 9F) as a result of coalescence of kinetically trapped nonequilibrium spheres, as formed

off-chip (Figure 9E); this suggests that under chemical conditions where off-chip structures are trapped away from equilibrium, on-chip shear may provide sufficient energy to allow micelles to move closer to their lowest-free energy morphology.

Although some vesicles are generated from spheres on-chip *via* Path 2 (Scheme 2) in the 15/85, cwc + 1 wt % case, the majority of micelles remain spherical (Figure 9B); however, by carrying out self-assembly in pure dioxane (0/100 composition) at cwc + 1 wt %, we have identified chemical conditions that generate no vesicles under off-chip equilibrium conditions (Figure 10A), but lead to either a majority of vesicles or a pure vesicle population on-chip (Figure 10B). The bulk morphology (Figure 10A) shows a mixture of spheres and flat lamellar structures, which are precursors to vesicles, indicating an equilibrium condition on the phase boundary between spheres and vesicles (Figure 4). Compared to the 15/85, cwc + 1 wt % case, where only a few shear-induced vesicles are generated on-chip, the presence of pure dioxane as the organic solvent appears to adjust the coalescence activation barrier (E_{a1}, Scheme 1) to a level that maximizes coalescence while at the same time minimizes fission in favor of intraparticle rearrangements, allowing pure vesicle populations to be generated. The kinetic effect of increasing the dioxane content would be to lower the core viscosity component of the coalescence activation barrier by increasing the degree of solvent swelling in the PS core; at the same time, increasing dioxane should increase the electrosteric activation energy, since the water content at the cwc is higher, leading to a higher concentration of water localized in the PAA corona and thus increasing the charge density of the brush.[40]

By increasing the water content to cwc + 2 wt % in dioxane, the equilibrium morphology moves into the vesicle region, and a pure population of vesicles is obtained off-chip (Figure 10C); on-chip, vesicles are also observed, although characterized by a population of very large vesicles (up to a micrometer in diameter) that apparently formed from the shear-induced coalescence of smaller vesicles (Figure 10D). Finally, at the highest water content of cwc + 4 wt %, a pure population of small vesicles is observed in the off-chip case (Figure 10E); the vesicles generated in the same chemical conditions on-chip are very similar in size, although they are accompanied by a population of spherical micelles that are not present in the bulk (Figure 10F). These spheres may have formed as a result of shear-induced breakup of some of the small vesicles that form upon water mixing; another possibility is that they represent trapped transition structures that are locked in during vesicle formation as a result of the fast on-chip mixing.

In summary, the interplay of chemical and shear forces on chip can be categorized in terms of three main paths for on-chip morphological transitions under different conditions of solvent composition and water content: Path 1, sphere-to-cylinder transition *via* shear-induced coalescence (*e.g.*, on-chip self-assembly at dioxane contents up to 35/65 DMF/dioxane); Path 2, sphere-to-vesicle transition *via* shear-induced coalescence (*e.g.*, 15/85 DMF/dioxane, cwc + 1 wt %; 0/100 DMF/dioxane, cwc + 1.0 wt %). Path 1 and Path 2 both follow the energy diagram represented in Scheme 1, with the main difference being the morphology that forms as a result of intraparticle rearrangement, which we have shown depends on the proximity of the initial equilibrium state to other morphological regions on the phase diagram. Finally, Path 3, cylinder-to-sphere transition *via* shear-induced breakup under high capillary number conditions (*e.g.*, 15/85 DMF/dioxane, cwc + 2 wt %). The determination of operative conditions for these various on-chip pathways, demonstrated here, highlights the immense potential of on-chip self-assembly as a means of combining chemical forces with shear processing to effect fine control over nanoscale colloidal structure.

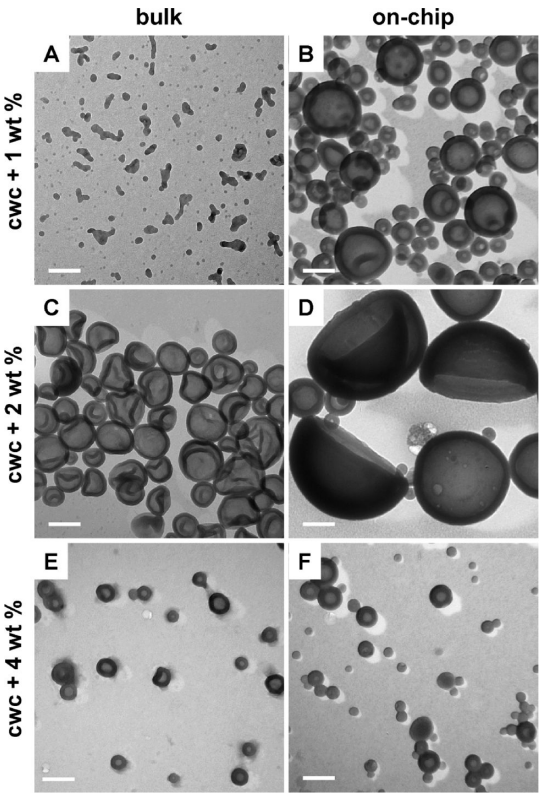

Figure 10. Effect of water content on off-chip and on-chip morphologies of PS(665)-*b*-PAA(68) in dioxane. TEM images of micelle morphologies formed from bulk (A,C,E) and on-chip (B,D,F) self-assembly of PS(665)-*b*-PAA(68) (c_0 = 0.33 wt %) in dioxane at water contents of cwc + 1.0 wt % (A,B), cwc + 2.0 wt % (C,D), and cwc + 4.0 wt % (E,F). For this solvent system, cwc = 8.5 ± 0.1 wt %. The on-chip flow rate is Q = ~5 μL/min. The scale bars indicate 200 nm.

Polymer Concentration and Added Salt Dependence of On-Chip PS-*b*-PAA Morphologies. In the previous section, differences in on-chip morphologies with variation in solvent composition or water content were mainly attributed to thermodynamic, rather than kinetic effects.

By contrast, in this section we investigate the effect of polymer concentration and salt addition on the on-chip morphology, and find dramatic morphology differences that we attribute mainly to increased rates of coalescence, suggesting morphology differences as a result of differences in kinetics rather than thermodynamics.

In Figure 11, we compare off-chip and on-chip morphologies for the 75/25 DMF/dioxane, cwc + 2 wt % system at two different polymer concentrations: our standard concentration of $c_0 = 0.33$ wt % and an elevated polymer concentration 3× higher: $c_0 = 1.0$ wt %. Note that the $c_0 = 0.33$ wt % condition is identical to that in the off-chip and on-chip experiments described previously (Figure 7C,D). As well, it is important to mention that while in general cwc values show some dependence on the polymer concentration,[16] the measured cwc values at $c_0 = 0.33$ wt % and $c_0 = 1.0$ wt % were in fact identical within experimental error, so that the water contents for the two experiments were also identical.

At both polymer concentrations, the off-chip experiments yield spherical micelles (Figure 11A,C), indicating that polymer concentration does not have an influence on the off-chip micelle morphology in this range. However, on-chip, the morphologies are dramatically different at the two polymer concentrations. A discussed previously, the lower polymer concentration yields a mixture of spheres and shear-induced branched cylinders and cylinder networks, along with a few lamellae (Figure 11B). On the other hand, the higher polymer concentration generates surprising and impressively large extended aggregates (Figure 11D), which consist of an interconnected network of large lamellar sheets. In some cases, these large bilayer networks, which we term "dinosomes" (similar aggregates have also been called large compound vesicles elsewhere in the literature),[11] extend for several micrometers and often appear broken or damaged by sample preparation and water evaporation, indicative of the large volumes of water that were encapsulated by the extensive bilayer sheets in the colloid state.

Although block copolymer concentration is known to influence the equilibrium morphology of block copolymer micelles, the effect is generally quite weak, as obviated by the very steep morphological phase boundaries in the polymer concentration−water content phase diagram determined for the PS(310)-*b*-PAA(52) copolymer in dioxane/water mixtures.[21] This weak thermodynamic effect, in addition to the large size difference in the aggregates obtained at the two polymer concentrations, suggests that the most important result of increasing the copolymer concentration is to increase the concentration of micelles and thus increase the on-chip collision/coalescence rate dramatically. As a result, a much larger number of primary spherical micelles effectively coalesce into a single giant aggregate as the liquid plugs travel through the chip, with the resulting bilayer structure

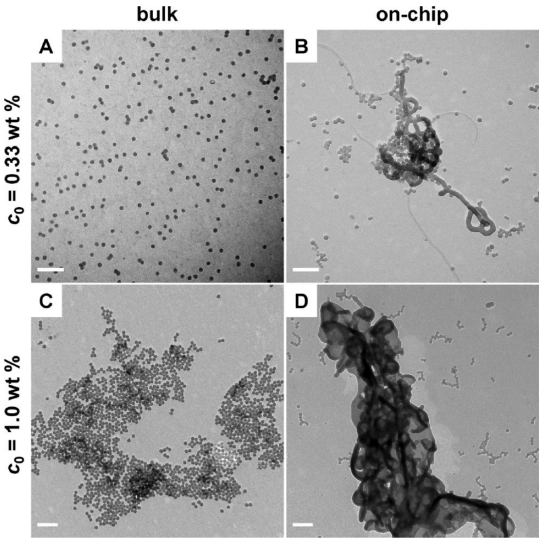

Figure 11. Effect of initial polymer concentration on off-chip and on-chip morphologies of PS(665)-*b*-PAA(68) in 75/25 (w/w) DMF/dioxane. TEM images of micelle morphologies formed from bulk (A,C) and on-chip (B,D) self-assembly of PS(665)-*b*-PAA(68) at two different polymer concentrations: $c_0 = 0.33$ wt % (A,B) and $c_0 = 1.0$ wt % (C,D). For all experiments, the solvent system is 75/25 (w/w) DMF/dioxane at a water content of cwc + 2.0 wt %. The on-chip flow rate is $Q = \sim 5$ μL/min. The scale bars indicate 200 nm.

governed by the resulting high local concentration of copolymer chains. Thus we view the demonstrated polymer concentration effect on the on-chip morphology to be kinetic, rather than thermodynamic, in origin.

Interestingly, we can effect a very similar morphology change on-chip to that obtained by increasing the polymer concentration by adding a small amount of salt ($R_{NaCl} = 0.2$ mol NaCl per mol acrylic acid repeat unit) to the self-assembly mixture prior to inducing micellization by adding water above the cwc. In both off-chip and on-chip experiments, the salt was added to the DMF/dioxane/copolymer solution *via* a concentrated 0.2 M NaCl aqueous solution, resulting in an initial water content well below the cwc; the remaining water was then added either dropwise off-chip or *via* mixing with the water-containing stream on-chip. Again, all experiments were carried out for the solvent condition 75/25 DMF/dioxane, cwc + 2 wt %, where the measured cwc with and without salt at $R_{NaCl} = 0.2$ was found to be identical within experimental error. The off-chip and on-chip morphologies with and without added salt are shown in Figure 12. Off-chip, the small amount of added salt does not influence the morphology, with spheres observed in both cases (Figure 12A,C). Eisenberg and co-workers have studied the influence of added salt on the morphologies of PS-*b*-PAA block copolymers,[11,16,22,34] and observed dramatic morphology transitions, but only for salt contents $R_{NaCl} > 0.4$;[11] therefore, the spheres we observe *via* off-chip self-assembly both with and without added salt are consistent with their results. On-chip, the added salt gives rise to similar dinosome aggregates (although not

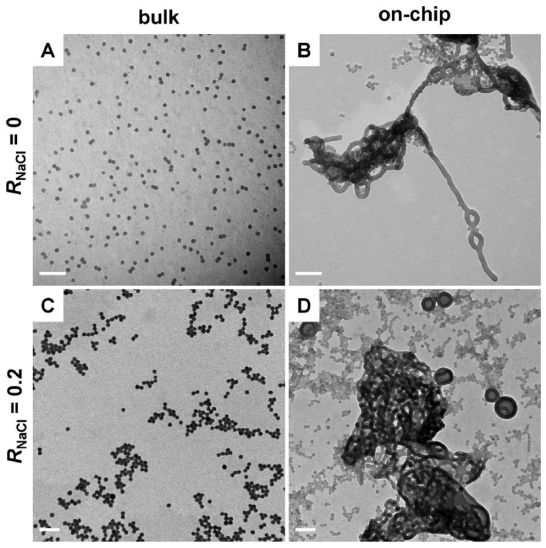

Figure 12. Effect of added salt on off-chip and on-chip morphologies of PS(665)-*b*-PAA(68) in 75/25 (w/w) DMF/dioxane. TEM images of micelle morphologies formed from bulk (A,C) and on-chip (B,D) self-assembly of PS(665)-*b*-PAA(68) (c_0 = 0.33 wt %) with salt added at a molar ratio per acrylic acid group of R_{NaCl} = 0 (no salt, A,B) and R_{NaCl} = 0.2 (C, D). For all experiments, the solvent system is 75/25 (w/w) DMF/dioxane at a water content of cwc + 2.0 wt %. The on-chip flow rate is Q = ~5 μL/min. The scale bars indicate 200 nm.

as large) to those obtained at elevated polymer concentration, along with vesicles (Figure 12D), in contrast to the cylindrical aggregates generated on-chip without added salt (Figure 12B).

The observed effect of added salt on the on-chip morphologies can be explained by a combination of kinetic and thermodynamic effects. Similar to increasing the polymer concentration, the addition of salt will increase the rate of on-chip coalescence events, not by increasing the collision rate, as in the case of elevated polymer concentration, but by decreasing the electrosteric contribution to the activation barrier E_{a1} (Scheme 1). The short-range electrosteric repulsion between charged polymer brushes has previously been shown to decrease as the ionic strength increases,[44] leading in the present case to an increased rate of successful collisions with added salt. As a result of this increased rate of coalescence, similar large dinosome structures are generated to those observed at the higher polymer concentration. In addition to this kinetic effect, adding salt has been shown by Eisenberg and co-workers to change the free energy of the self-assembling system by effectively screening electrostatic repulsive interactions between proximal charged PAA chains, leading to morphological transitions from spheres to cylinders to vesicles as the salt content is increased.[11,16,22,34] As well, changes in the solvent quality of nonionic PS blocks in polar DMF with added salt cannot be ruled out.[45] Although the weak salt effects present at R_{NaCl} = 0.2 are not significant enough to effect a change in morphology off-chip, they do change the equilibrium position of the system, effectively moving the spherical micelles closer to the vesicle region of an appropriate phase diagram. Thus, when coalescence induces increases in aggregation number, the resulting intraparticle rearrangements to locally minimize free energy give rise to vesicles (Figure 12D), rather than the cylinders formed in the absence of added salt (Figure 12C).

Conclusions. We have investigated the effect of various chemical conditions (solvent composition, water content, polymer concentration, and added salt) on the morphologies formed by PS-*b*-PAA in DMF/dioxane/water mixtures on a two-phase gas−liquid segmented microfluidic reactor. The resulting morphological trends are explained by the interplay of top-down shear effects (coalescence and breakup) and bottom-up chemical forces. Using off-chip morphology results, an equilibrium phase diagram of the present block copolymer system in various DMF/dioxane/water mixtures was constructed. In many cases, the on-chip morphologies could be explained by one of three identified shear-induced paths which depended on the initial equilibrium positions on the phase diagram. In addition, polymer concentration and salt content were found to have a dramatic kinetic effect on micelle morphology when combined with on-chip shear forces, due to the increased rate of coalescence that was effected by changes in these parameters. Top-down directed molecular self-assembly in microfluidic devices offers immense potential for a variety of applications, as it promises new and convenient handles on colloidal morphology and size at the nanoscale.

METHODS

Materials. The composition of the polystyrene-*block*-poly(acrylic acid) sample used in this study was PS(665)-*b*-PAA(68). Anionic polymerization was employed to synthesize the associated polystyrene-*block*-poly(*tert*-butyl acrylate) block copolymer, followed by hydrolysis of the ester block. The numbers in parentheses refer to number-average degrees of polymerization of each block. The reagents, dimethylformamide (DMF) (Aldrich, 99.9+%, HPLC grade, H_2O < 0.03%) and 1,4-dioxane Aldrich, 99.0%, reagent grade, H_2O < 0.05% were used as received without further purification.

Critical Water Content Determination. Static light scattering measurements were carried out in order to accurately determine the critical water content (cwc) of PS(665)-*b*-PAA(68) for different chemical variables (polymer concentrations, solvent mixtures and salt contents) applied in this study. Light scattering experiments were performed on a Brookhaven Instruments photon correlation spectrometer equipped with a BI-200SM goniometer, a BI-9000AT digital autocorrelator, and a Melles Griot He−Ne Laser (632.8 nm) with a maximum power output of 75 mW. For instance, to determine the cwc of 0.33 wt % PS(665)-*b*-PAA(68) in pure DMF, stock solution was prepared by adding DMF solvent to a copolymer concentration of 0.66 wt %. The stock solution was then filtered through a Teflon syringe membrane filter with a nominal pore size of 0.45 μm (National Scientific Company) into precleaned scintillation vials. Next, the stock solution was diluted with DMF

solvent mixture filtered through two Teflon syringe filters with a nominal pore size of 0.20 μm (National Scientific Company) connected in series to give a polymer concentration of 0.33 wt %. Deionized water was next added dropwise to ~6 g of the solution in successive 0.02−0.05 g quantities *via* a microsyringe equipped with a membrane filter (Life Sciences) with a nominal pore size of 0.20 μm. After each addition of water, the solution was agitated with a vortexer to aid mixing. The scattered light intensity was recorded 15 min after vortexing to allow the solution to equilibrate. All measurements were carried out at a scattering angle of 90° and a temperature of 23 °C. The cwc thus obtained for DMF (Figure 2) was 2.8 ± 0.1 wt %. The cwc determinations of other solvent mixtures were carried out in similar fashion.

We also carried out cwc determinations for solutions under different chemical conditions, such as different polymer concentration and salt contents. For both of these measurements, the solvent mixture was 75/25 w/w DMF/dioxane which serves as a basis for comparisons. To determine the cwc for 1.0 wt % of PS(665)-*b*-PAA(68) in 75/25 w/w DMF/dioxane, a stock solution of 2 wt % copolymer in 75/25 w/w DMF/dioxane was used. It was diluted down to 1.0 wt % copolymer solution in 75/25 w/w DMF/dioxane using similar method. The cwc determination for the added salt effect in 75/25 w/w DMF/dioxane was carried out using stock solution of 0.66 wt % copolymer. The stock solution was treated with filtered 0.2 M NaCl solution in deionized water until the salt contents of 20% equivalent of the poly(acrylic acid) unit (R = 0.20) was added. Then the stock solution was diluted down to 0.33 wt % with filtered 75/25 w/w DMF/dioxane for the cwc measurement.

Off-Chip Micelle Preparation. Morphologies formed on-chip under different chemical and flow conditions were compared to off-chip control experiments in which block copolymer micelles were prepared in the following manner. Three water contents (cwc + 1, 2, and 4 wt % water) were investigated for each solvent composition. For instance, to prepare off-chip micelle solution in pure DMF, water contents of 1, 2, and 4 wt % above its respective cwc were used. To the three vials, each containing ~5 mL of 0.33 wt % PS(665)-*b*-PAA(68) in DMF, deionized water was added dropwise at a rate of 20 μL every 10 s with moderate magnetic stirring (600 rpm) until the various target water concentrations were reached (1, 2, and 4 wt % above cwc). The resulting micelles were then allowed to equilibrate for 2 weeks without stirring, followed by kinetic trapping *via* fast transfer into ~50 mL of deionized water. The colloidal dispersions were finally dialyzed against deionized water to remove residual organic solvent.

Microfluidic Chip Fabrication. High-quality silicon wafers (Silicon Quest International, CA) and negative photoresist, SU-8 100 (Microchem Inc., MA) were used to fabricate negative masters. Prior to use, new silicon wafers were heated on a hot plate to at 200 °C for 20 min to remove all moisture. SU-8 films (150 μm thick) were spin-coated onto the silicon wafers, followed by heating at 95 °C for 60 min to remove residual SU-8 solvent. A photomask was placed over the film for exposure under UV light for 180 s. The device was heated for an additional 20 min at 95 °C. After that, the device was submerged in SU-8 developer (Microchem, MA) until all unexposed photoresist was removed. The reactor has a set channel depth of 150 μm, and consists of a sinusoidal mixing channel 100 μm wide and 100 mm in length and a sinusoidal processing channel 200 μm wide and 740 mm in length.

To further stabilize the process of bubble generation, we employed external resistor chips, which were connected in series between the Ar gas tank and the microfluidic chip. These resistors were 1000 mm long, 400 μm wide, and 150 μm deep. In operation, these high pressure drop resistors serve to effectively dampen the pressure fluctuations caused by the Ar gas tank and the bubble generation process itself. The resistors were designed in a way that the total pressure drop in the resistors was at least 1 order of magnitude higher than the pressure drop in the reaction channel.

Microfluidic chips were fabricated from poly(dimethylsiloxane) (PDMS) using a SYLGARD 184 silicon elastomer kit (Dow Corning, MI) with an elastomer base-to-curing agent ratio of 10:1. The elastomer and curing agent were mixed together and degassed in a vacuum chamber. The degassed PDMS was poured onto the negative master in a Petri dish and then degassed again until all remaining air bubbles in the PDMS were removed. The PDMS was then heated at 85 °C until cured (~50 min). The microfluidic chips were cut and peeled off the master, and holes were punched through its reservoirs to allow for the insertion of tubing. A thin PDMS film was formed on a glass slide by spin-coating and was permanently bonded to the base of the microfluidic reactor after both components were exposed to oxygen plasma for 30 s.

Flow Delivery and Control. The pressure-driven flow of liquids to the inlets of the reactors was provided using 250 μL and 1 mL gastight syringes (Hamilton, NV) mounted on syringe pumps (Harvard Apparatus, MA). The microchip was connected to the syringes with 1/16th inch (o.d.) Teflon tubing (Scientific Products and Equipment, ON). Gas pressure was adjusted by a Ar tank regulator as well as a downstream regulator for fine adjustments (Johnson Controls Inc.). For gas flow, connections were joined using Teflon tubing of 1/16 in. (o.d.) and 100 μm (i.d.) (Upchurch Scientific, WA). The liquid flow rate (Q_{liq}) was programmed *via* the syringe pumps and the gas flow rate (Q_{gas}) was varied by tuning the pressure regulator. For all experiments in this paper, the nominal relative gas-to-liquid flow ratio (Q_{gas}/Q_{liq}.) was ~1, and a single nominal total flow rate was investigated: Q_{total} = ~5 μL/min (low flow rate case). Because of the compressible nature of the gas and the high gas/liquid interfacial tension, discrepancies arise between the nominal (programmed) and actual values of Q_{gas}, Q_{gas}/Q_{liq}, and the total flow rate (Q_{total}). Therefore, actual gas flow rates were calculated from the frequency of bubble formation and the average volume of gas bubbles, determined from image analysis of the mean lengths of liquid and gas plugs, L_{liq} and L_{gas}, respectively, under a given flow set of conditions (Supporting Information, Table S1). This method of flow determination has been previously employed in the context of gas−liquid multiphase flow in microfluidic devices.[43]

On-Chip Micelle Preparation. For microfluidic self-assembly experiments, three separate liquid streams were combined at an equal flow rate to form gas-separated liquid plugs within the reactor: (1) a 1.0 wt % solution of PS(665)-*b*-PAA(68) single chains in DMF/dioxane, (2) a separator stream containing DMF/dioxane only; and (3) a solution of DMF/dioxane containing differing deionized water contents. The particular DMF/dioxane w/w ratio depends on the individual runs. A combination of the three liquid streams yielded steady-state on-chip concentrations of 0.33 wt % polymer, identical to the off-chip control experiments, and either 1.0, 2.0, and 4.0 wt % above the cwc, respectively. Microfluidic flow conditions were selected as described in the previous section.

For off-chip analysis of micelle morphologies prepared within the reactor, micellar dispersions were generally collected from the chip following the processing channel into vials containing a large excess (~250 μL) of deionized water, where the particles immediately became kinetically frozen due to the high water content. The solids content of the final mostly aqueous solution was ~0.25 mg/mL.

Flow visualization of microfluidic experiments and quantification of all the flow conditions were performed with an inverted fluorescence microscopy system operating in transmission mode. Optical images of the reactor were capture using a CCD camera (AF6000 Orca, Hamamatsu, NJ) installed on the inverted microscope (DMI 6000B, LEICA, NJ).

TEM and Image Analysis. Transmission electron microscopy (TEM) of various aqueous micellar dispersions was performed with a Hitachi H-7000 electron microscope operating at 75 kV and a JEOL JEM-1400 microscope operating 80 kV. For TEM imaging, a 10 μL drop of micellar dispersion was deposited onto either a carbon-coated or carbon-coated Formvar 300 mesh copper grid, and then shadowed with Pt/Pd wire for imaging. For TEM imaging of on-chip prepared samples, the small quantity of dioxane remaining in the final solutions was found to dissolve Formvar substrates, and so carbon-coated grids without Formvar were required for these samples.

Analysis of micellar features (sphere diameter, cylinder diameter, vesicle wall thickness, *etc.*) were carried on images randomly

selected from various regions of the TEM grid. They were measured from printouts of multiple regions of the TEM grid where the particles appeared 40000 to 50000 times their actual size.

Conflict of Interest: The authors declare no competing financial interest.

Acknowledgment. The authors are grateful for the financial support of the Natural Sciences and Engineering Research Council (NSERC) of Canada, through research grants to D.S. and M.G.M. Infrastructure funding from the Canada Foundation for Innovation (CFI) and British Columbia Knowledge Development Fund (BCKDF) is also gratefully acknowledged, along with a Collaborative Research Stipend from the Centre for Advanced Materials and Related Technologies (CAMTEC, UVic).

Supporting Information Available: Actual measured flow data for various microfluidic experiments described in the text. This material is available free of charge *via* the Internet at http://pubs.acs.org.

REFERENCES AND NOTES

1. Discher, B. M.; Won, Y.-Y.; Ege, D. S.; Lee, J. C.-M.; Bates, F. S.; Discher, D. E.; Hammer, D. A. Polymersomes: Tough Vesicles Made from Diblock Copolymers. *Science* **1999**, *284*, 1143–1146.
2. Jain, S.; Bates, F. S. On the Origins of Morphological Complexity in Block Copolymer Surfactants. *Science* **2003**, *300*, 460–464.
3. Jain, S.; Bates, F. S. Consequences of Nonergodicity in Aqueous Binary PEO−PB Micellar Dispersions. *Macromolecules* **2004**, *37*, 1511–1523.
4. Won, Y. Y.; Davis, H. T.; Bates, F. S. Giant Wormlike Rubber Micelles. *Science* **1999**, *283*, 960–963.
5. Cui, H.; Chen, Z.; Zhong, S.; Wooley, K. L.; Pochan, D. J. Block Copolymer Assembly *via* Kinetic Control. *Science* **2007**, *317*, 647–650.
6. Cui, H. G.; Chen, Z. Y.; Wooley, K. L.; Pochan, D. J. Origins of Toroidal Micelle Formation through Charged Triblock Copolymer Self-assembly. *Soft Matter* **2009**, *5*, 1269–1278.
7. Li, Z. B.; Chen, Z. Y.; Cui, H. G.; Hales, K.; Qi, K.; Wooley, K. L.; Pochan, D. J. Disk Morphology and Disk-to-Cylinder Tunability of Poly(acrylic acid)-*b*-poly(methyl acrylate)-*b*-polystyrene Triblock Copolymer Solution-State Assemblies. *Langmuir* **2005**, *21*, 7533–7539.
8. Li, Z.; Chen, Z.; Cui, H.; Hales, K.; Wooley, K. L.; Pochan, D. J. Controlled Stacking of Charged Block Copolymer Micelles. *Langmuir* **2007**, *23*, 4689–4694.
9. Zhang, L.; Eisenberg, A. Multiple Morphologies of Crew-Cut Aggregates of Polystyrene-*b*-poly(acrylic acid) Block-Copolymers. *Science* **1995**, *268*, 1728–1731.
10. Zhang, L.; Eisenberg, A. Multiple Morphologies and Characteristics of "Crew-Cut" Micelle-like Aggregates of Polystyrene-*b*-poly(acrylic acid) Diblock Copolymers in Aqueous Solutions. *J. Am. Chem. Soc.* **1996**, *118*, 3168–3181.
11. Zhang, L.; Eisenberg, A. Morphogenic Effect of Added Ions on Crew-Cut Aggregates of Polystyrene-*b*-poly(acrylic acid) Block Copolymers in Solutions. *Macromolecules* **1996**, *29*, 8805–8815.
12. Yu, K.; Zhang, L.; Eisenberg, A. Novel Morphologies of "Crew-Cut" Aggregates of Amphiphilic Diblock Copolymers in Dilute Solution. *Langmuir* **1996**, *12*, 5980–5984.
13. Shen, H.; Zhang, L.; Eisenberg, A. Thermodynamics of Crew-Cut Micelle Formation of Polystyrene-*b*-poly(acrylic acid) Diblock Copolymers in DMF/H_2O Mixtures. *J. Phys. Chem. B* **1997**, *24*, 4697–4708.
14. Yu, Y.; Eisenberg, A. Control of Morphology through Polymer−Solvent Interactions in Crew-Cut Aggregates of Amphiphilic Block Copolymers. *J. Am. Chem. Soc.* **1997**, *119*, 8383–8384.
15. Yu, Y. S.; Zhang, L.; Eisenberg, A. Multiple Morphologies of Crew-Cut Aggregates of Polybutadiene-*b*-poly(acrylic acid) Diblocks with Low T_g Cores. *Langmuir* **1997**, *13*, 2578–2581.
16. Zhang, L.; Shen, H.; Eisenberg, A. Phase Separation Behavior and Crew-Cut Micelle Formation of Polystyrene-*b*-poly(acrylic acid) Copolymers in Solutions. *Macromolecules* **1997**, *30*, 1001–1011.
17. Yu, G. E.; Eisenberg, A. Multiple Morphologies Formed from an Amphiphilic ABC Triblock Copolymer in Solution. *Macromolecules* **1998**, *31*, 5546–5549.
18. Yu, K.; Bartels, C.; Eisenberg, A. Vesicles with Hollow Rods in the Walls: A Trapped Intermediate Morphology in the Transition of Vesicles to Inverted Hexagonally Packed Rods in Dilute Solutions of PS-*b*-PEO. *Macromolecules* **1998**, *31*, 9399–9402.
19. Yu, K.; Eisenberg, A. Bilayer Morphologies of Self-Assembled Crew-Cut Aggregates of Amphiphilic PS-*b*-PEO Diblock Copolymers in Solution. *Macromolecules* **1998**, *31*, 3509–3518.
20. Yu, Y.; Zhang, L.; Eisenberg, A. Morphogenic Effect of Solvent on Crew-Cut Aggregates of Amphiphilic Diblock Copolymers. *Macromolecules* **1998**, *31*, 1144–1154.
21. Shen, H.; Eisenberg, A. Morphological Phase Diagram for a Ternary System of Block Copolymer PS_{310}-*b*-PAA_{52}/Dioxane/H_2O. *J. Phys. Chem. B* **1999**, *103*, 9473–9487.
22. Shen, H.; Zhang, L.; Eisenberg, A. Multiple pH-Induced Morphological Changes in Aggregates of Polystyrene-*block*-poly(4-vinylpyridine) in DMF/H_2O Mixtures. *J. Am. Chem. Soc.* **1999**, *121*, 2728–2740.
23. Yu, K.; Bartels, C.; Eisenberg, A. Trapping of Intermediate Structures of the Morphological Transition of Vesicles to Inverted Hexagonally Packed Rods in Dilute Solutions of PS-*b*-PEO. *Langmuir* **1999**, *15*, 7157–7167.
24. Zhang, L.; Eisenberg, A. Crew-Cut Aggregates from Self-Assembly of Blends of Polystyrene-*b*-poly(acrylic acid) Block Copolymers and Homopolystyrene in Solution. *J Polym. Sci. B: Polym. Phys.* **1999**, *37*, 1469–1484.
25. Zhang, L.; Eisenberg, A. Thermodynamic *vs* Kinetic Aspects in the Formation and Morphological Transitions of Crew-Cut Aggregates Produced by Self-Assembly of Polystyrene-*b*-poly(acrylic acid) Block Copolymers in Dilute Solution. *Macromolecules* **1999**, *32*, 2239–2249.
26. Lim Soo, P.; Eisenberg, A. Preparation of Block Copolymer Vesicles in Solution. *J Polym. Sci. B: Polym. Phys.* **2004**, *42*, 923–938.
27. Choucair, A.; Eisenberg, A. Control of Amphiphilic Block Copolymer Morphologies Using Solution Conditions. *Eur. Phys. J. E* **2003**, *10*, 37–44.
28. Allen, C.; Maysinger, D.; Eisenberg, A. Nano-engineering Block Copolymer Aggregates for Drug Delivery. *Colloid Surf. B* **1999**, *16*, 3–27.
29. Geng, Y.; Dalhaimer, P.; Cai, S.; Tsai, R.; Tewari, M.; Minko, T.; Discher, D. E. Shape Effects of Filaments *versus* Spherical Particles in Flow and Drug Delivery. *Nat. Nanotechnol.* **2007**, *2*, 249–255.
30. Gonzalez, D. C.; Savariar, E. N.; Thayumanavan, S. Fluorescence Patterns from Supramolecular Polymer Assembly and Disassembly for Sensing Metallo- and Nonmetalloproteins. *J. Am. Chem. Soc.* **2009**, *131*, 7708–7716.
31. Torchilin, V. P. PEG-based Micelles as Carriers of Contrast Agents for Different Imaging Modalities. *Adv. Drug Delivery Rev.* **2002**, *54*, 235–252.
32. Nasongkla, N.; Bey, E.; Ren, J. M.; Ai, H.; Khemtong, C.; Guthi, J. S.; Chin, S. F.; D., S. A.; Boothman, D. A.; Gao, J. M. Multifunctional Polymeric Micelles as Cancer-Targeted, MRI-Ultrasensitive Drug Delivery Systems. *Nano Lett.* **2006**, *6*, 2427–2430.
33. Wu, W. C.; Chen, C. Y.; Tian, Y. Q.; Jang, S. H.; Hong, Y. N.; Liu, Y.; Hu, R. R.; Tang, B. Z.; Lee, Y. T.; Chen, C. T.; *et al.* Enhancement of Aggregation-Induced Emission in Dye-Encapsulating Polymeric Micelles for Bioimaging. *Adv. Funct. Mater.* **2010**, *20*, 1413–1423.
34. Zhang, L.; Yu, K.; Eisenberg, A. Ion-Induced Morphological Changes in "Crew-Cut" Aggregates of Amphiphilic Block Copolymers. *Science* **1996**, *272*, 1777–1779.
35. Mendes, E.; Narayanan, J.; Oda, R.; Kern, F.; Candau, S. J.; Manohar, C. Shear-Induced Vesicle to Wormlike Micelle Transition. *J. Phys. Chem. B* **1997**, *101*, 2256–2258.

36. Wang, J. F.; Chen, Q. J.; Zhao, H.; Ming, T.; Wu, C. Nanopore Extrusion-Induced Transition from Spherical to Cylindrical Block Copolymer Micelles. *J. Am. Chem. Soc.* **2009**, *131*, 16650–16651.
37. Zhang, M.; Wang, M. F.; He, S.; Qian, J. S.; Saffari, A.; Lee, A.; Kumar, S.; Hassan, Y.; Guenther, A.; Scholes, G.; Winnik, M. A. Sphere-to-Wormlike Network Transition of Block Copolymer Micelles Containing CdSe Quantum Dots in the Corona. *Macromolecules* **2010**, *43*, 5066–5074.
38. Wang, Z.; Jiang, W. Effect of Shear Flow on the Self-Assembly of ABC Triblock Copolymers in Selective Solvent. *Chem. Phys. Lett.* **2010**, *487*, 84–87.
39. Hayward, R. C.; Pochan, D. J. Tailored Assemblies of Block Copolymers in Solution: It Is All about the Process. *Macromolecules* **2010**, *43*, 3577–3584.
40. Wang, C.-W.; Sinton, D.; Moffitt, M. G. Flow-Directed Block Copolymer Micelle Morphologies *via* Microfluidic Self-Assembly. *J. Am. Chem. Soc.* **2011**, *133*, 18853–18864.
41. Wang, C.-W.; Bains, A.; Sinton, D.; Moffitt, M. G. Flow-Directed Assembly of Block Copolymer Vesicles in the Lab-on-a-Chip. *Langmuir* **2012**, *28*, 15756–15761.
42. Schabas, G.; Wang, C.-W.; Oskooei, A.; Yusuf, H.; Moffitt, M. G.; Sinton, D. Formation and Shear-Induced Processing of Quantum Dot Colloidal Assemblies in a Multiphase Microfluidic Chip. *Langmuir* **2008**, *24*, 10596–10603.
43. Wang, C.-W.; Oskooei, S. A. K.; Sinton, D.; Moffitt, M. G. Controlled Self-Assembly of Quantum Dot-Block Copolymer Colloids in Multiphase Microfluidic Reactors. *Langmuir* **2010**, *26*, 716–723.
44. Carambassis, A.; Rutland, M. W. Interactions of Cellulose Surfaces: Effect of Electrolyte. *Langmuir* **1999**, *15*, 5584–5590.
45. von Hippel, P. H.; Wong, K.-Y. Neutral Salts: The Generality of their Effects on the Stability of Macromolecular Conformations. *Science* **1964**, *145*, 577–580.